Cappelli, A., and M. Dente, "Application of a Nonlinear Evaluation Method to the Analysis of Kinetic Data from an Integral Reactor," *Chim. E. Ind.*, **47**, 1068 (1965).
Carberry, J. J., "Chemical and Catalytic Reaction Engineering," McGraw-Hill (1976).
Carra, S., and L. Forni, "Aspetti Cinetici delta Teoria del Reatore-Chimico," Tamburini, Milan (1974).
Cropley, J. B., "Heuristic Approach to Complex Kinetics," *ACS Symp. Ser.*, **65**, 292 (1978).
Damköhler, G., "Einflüsse der Strömung, Diffusion und des Wärmeüberganges auf die Leistung von Reaktionsofen," *Z. Elektrochem.*, **42**, No. 12, 846 (1936).
Damköhler, G., *Der Chemie—Ingenieur* **III**, Part One, 447 (1937).
Frank-Kamenetskii, D. A., "Ignition of Coal and High-Speed Gasification," *J. Tech. Phys.*, (USSR) **9**, 1457 (1939).
Frank-Kamenetskii, D. A., "Diffusion and Heat Transfer in Chemical Kinetics," Plenum Press, 2nd ed. (1961).
Froment, G. E., and K. B. Bischoff, "Chemical Reactor Analysis and Design," John Wiley (1976).
Gilles, E. D., and H. Hofmann, "Bermerkung zu der Arbeit: An Analysis of Chemical Reactor Stability and Control," *Chem. Eng. Sci.*, **5**, 328 (1961).
ICI, "Low-Cost, Low-Pressure Methanol," *Chem. Eng.*, 86 (Dec. 1, 1969).
Kung, H. H., "Methanol Synthesis," *Catal. Rev.—Sci. Eng.*, **22** (2), 235 (1980).
Liljenroth, F. G., "Starting and Stability Phenomena of Ammonia-Oxidation and Similar Reactions," *Chem. Met. Eng.*, **19**, 287 (1918).
Luss, D., Professional Progress Award Lecture, 73rd Annual Meeting of AIChE, Chicago, IL (Nov. 10–20, 1980).
Natta, G., "Synthesis of Methanol," *Catalysis*, P. H. Emmett, ed., **3**, 345, Reinhold, NY (1955).
Parekh, V. J., "Preliminary Kinetic Study of the Low-Pressure Methanol Synthesis," M.S. Thesis, Univ. of Akron, Akron, OH (1980).
Perkins, G. A., Carbide and Carbon Chemical Corp., Weekly Progress Report 3/15 (1938).
Perlmutter, D. D., "Stability of Chemical Reactors," Prentice-Hall, Inc. (1972).
Schmitz, R. A., "Multiplicity, Stability and Sensitivity of States in Chemically Reacting Systems—A Review," *Advances in Chemistry Series*, **148**, Chem. Reaction Eng. Reviews (1975).
Schmitz, R. A., R. R. Bautz, W. E. Ray, and A. Uppal, "The Dynamic Behavior of a CSTR: Some Comparisons of Theory and Experiment," *AIChE J.*, **25**, No. 2, 289 (March 1979).
Shinnar, R., "Chemical Reactor Modeling—The Desirable and the Achievable," *ACS Symp. Ser.* No. 72 (1978).
Stephens, A. D., "Stability and Optimization of a Methanol Converter," *Chem. Eng. Sci.*, **30**, 11 (1975).
Uppal, A., W. H. Ray, and A. B. Poore, "On the Dynamic Behavior of Continuous Stirred Tank Reactors," *Chem. Eng. Sci.*, **29**, 967 (1974).
Uppal, A., W. H. Ray, and A. B. Poore, "The Classification of the Dynamic Behavior of Continuous Stirred Tank Reactors—Influence of Reactor Residence Time," **31**, 205 (1976).
Van Heerden, C., "Autothermic Processes—Properties and Reactor Design," *Ind. Eng. Chem.*, **45**, 1242 (1953).
Van Heerden, C., "The Character of the Stationary State of Exothermic Processes," Proc. of the 1st European Symposium on Chemical Reaction Engineering, p. 133, Amsterdam, Pergamon Press (1958).
Wagner, C., "Über die Temperature Einstellung an Hochstleistungskatalysatoren," *Chem. Tech.*, **18**, 28 (1945).
Weller, S. W., "Kinetic Models in Heterogeneous Catalysis," *Adv. in Chem. Ser.*, No. 148 (1976).
Wicke, E., and D. Vortmeyer, "Zündzonen heterogener Reaktionen in gasdurchströmten Körnerschichten," *Z. für Elektrochemie*, **63**, 145 (1959).
Wilson, K. B., "Tubular Reactors-Calculation and Analysis of Longitudinal Temperature Gradients in Tubular Reactors," *Trans. Inst. Chem. Eng.*, **24**, 77 (1946).
Zelenik, F. G., and S. Golden, "A General IBM 704 or 7090 Computer Program for Computation of Chemical Equilibrium Composition, Rocket Performance, and Chapman-Jouquet Detonations," NASA Technical Note, D-1454 (1962).

Manuscript received March 30, 1981; revision received December 17, and accepted January 13, 1982.

Time Dependence of Pressure In a Bubbler Tube

An experimental and theoretical study is presented of the time dependence of air pressure in a bubbler tube used to measure the liquid level in a tank. The observed time dependence of the air pressure is a superposition of two components. The first component is a repeated slow rise and sudden fall in the air pressure that is associated with bubble growth and breakoff. It is the sudden breakoff that generates the second component consisting of damped oscillations associated with sound waves in the air interacting with an oscillating flow of the liquid. The air pressure during bubble growth is described theoretically. This result is combined with the gas law to predict the functional form of the slow pressure rise; this prediction agrees with experiment. An equation for the oscillation frequencies is derived, solved, and compared with experiment; agreement is within the measurement accuracy of 5%.

A. K. GAIGALAS
and
BALDWIN ROBERTSON

Fluid Engineering Division
National Bureau of Standards
Washington, DC 20234

SCOPE

A widespread method for measuring the level of liquid contained in a tank uses a tube inserted down into the liquid and through which air (or nitrogen) is forced under pressure. The method is used in industry where a pressure transducer cannot be put inside the tank. Since the pressure necessary to force the air out of the lower end of the tube depends on the height of the liquid above the end of the tube, a measurement of the air pressure can be used to infer the height of the liquid. This can be used to determine the volume of liquid in the tank if the cross

Correspondence concerning this paper should be addressed to A. K. Gaigalas.

sectional area of the tank is known as a function of height. Calibration of a tank and the subsequent measurement of volume entail many uncertainties which have been described by Jones (1979) and Davies, et al. (1978). One of the problems encountered is the accurate determination of pressure. The nature of this problem will form the focus of the present paper.

Pressure measuring instruments are available with a resolution of 1 Pa out of 10^5 Pa full scale (10^5 Pa $\simeq$ 1 atm). Since 1 Pa corresponds to a height of water equal to about 0.1 mm, great accuracy in liquid height measurements can be attained if the pressure measurement can be made with an accuracy of 1 Pa. As the air is forced through the tube it escapes from the submerged end by forming bubbles. Whenever a bubble detaches itself from the end of the tube, the pressure in the tube varies dramatically with time. The instantaneous variation in pressure covers a range of approximately 80 Pa, which is very large compared with the desired measurement accuracy of 1 Pa. Consequently, it is important to understand the response of the air pressure to bubble formation and breakoff, for then it will be possible to optimize the accuracy of the pressure measurement by influencing the bubble formation process, as well as determining the best way of sampling the pressure signal.

CONCLUSIONS AND SIGNIFICANCE

The pressure variation in a bubbler tube was found to be a superposition of two distinct components, each traceable to a different physical mechanism. The first component, a slow pressure change between consecutive bubble breakoffs, was related to the development of the shape of the bubble and the air influx into the bubbler tube. By changing the geometry of the end of the bubbler tube, the bubble development was changed and consequently, the slow pressure variation was modified. The slow variation was largest for a bubbler tube with a slanted end which constrained the bubble growth to a direction parallel with the tube axis. The variation was least for a flanged end; here the bubble was free to grow horizontally.

Immediately following the bubble breakoff the pressure exhibits a fast damped oxcillation. This second component of the pressure variation was correlated through visual observation to the up-down motion of the air-liquid interface inside the bubbler tube. The frequency of the oscillation depends on the length of the bubbler tube, being 7 Hz for a 3.66 m tube and increasing as the tube is shortened. For longer tubes several oscillatory modes were superimposed to give a more complicated time dependence. It should be emphasized that the oscillations are damped and are confined to a small time interval following the bubble breakoff so that if the air influx into the tube is small, then the major portion of the time between bubble breakoffs is devoted to the slow pressure variation which is due to the bubble growth. If the air flow rate is large then the observed pressure variation becomes very complicated. We have observed that for large flow rate there is a substantial interaction between consecutive bubbles, that is, the oscillations due to the breakoff of one bubble affect the growth of the subsequent bubble. This interaction leads to complex but repeatable patterns in the pressure signal. In order to avoid this interaction, we set the bubble breakoff frequency in this study to a value much lower than the lowest resonant frequency.

The analysis of the bubble growth indicates that changes in the surface tension of the liquid influence the pressure in the tube in two ways. First, there is a change in the contribution from the "stretching" at the lowest point of the bubble, and second, the bubble grows differently in the horizontal direction and consequently changes its vertical dimension when the surface tension is changed. For water, a change of surface tension from 0.072 to 0.066 N/m lowers the maximum pressure in a 0.5 cm radius tube by 4 Pa. In practice, the sensitivity to surface tension change is reduced by using a tube with a larger diameter. The analysis of the pressure variation suggests that one way to make precise liquid level measurements is to use a flat-ended tube and sample the pressure after the damped oscillations have died down. Another way is to average the pressure over about 10 to 30 seconds in order to eliminate any dependence on the fast oscillations, whose average value is zero. Of course the slow variation will be averaged as well, and the value of this averaging depends on the time dependence of the pressure signal, which, as this study indicates, is not a sensitive function of the magnitude of the pressure. Either procedure leads to pressure readings repeatable to 1 Pa out of a mean pressure of 10^5 Pa even though the pressure variation is as large as 80 Pa.

INTRODUCTION

The bubble formation and breakoff process was studied experimentally. Data were accumulated for several tube diameters, tube lengths, and liquid levels. The general features of the process (observed in a 0.95 cm diameter tube with a flat end) are as follows. After the bubble has reached a certain size it suddenly breaks off from the tube in a time equal to $\simeq$ 0.02 s. With the bubble gone, the liquid moves back into the tube to a distance $\simeq$ 1 mm in a time $\simeq$ 0.02 s. The initial upward surge of the liquid is followed by damped oscillation of the liquid-air interface lasting for approximately 0.5 s. Meanwhile the average pressure in the tube increases slowly until a new bubble emerges. The accumulated data suggest that the damped oscillations and the slow pressure buildup are the two most important features which characterize the response of the tube to bubble detachment.

EXPERIMENTAL PROCEDURES

The experimental equipment, shown schematically in Figure 1, consisted of a 41-cm diameter iron tank, 365 cm high, a stainless steel bubbler tube immersed in the tank, a pressure transducer connected at the top of the bubbler tube, and electronic modules for pressure signal detection and recording. Data was taken for two bubbler tube diameters (0.95 cm and 1.91 cm) and several lengths. The length of the tube was varied by inserting pieces of hard plastic tubing between the 365 cm long stainless steel tube and the pressure transducer. When the length was changed, care was taken not to change the way the tube was connected to the transducer. Some of the data was taken using short glass tubes with the open lower end immersed in a 30-cm by 60-cm glass aquarium. Three lengths (17, 60, and 70 cm) of glass tubing were used to study and photograph bubble formation. The pressure was measured with a capacitive transducer (Datametrics 581 Barocell) and the accompanying electronic module. (Certain commercial equipment, instruments, or materials are identified in this paper in order to adequately specify the experimental procedure. In no case does such identification imply recommendation or endorsement by the National Bureau of Standards, nor does it imply that the material or equipment identified is necessarily the best available for the purpose.) The first mechanical resonance of the transducer is at 8 kHz, and the response of the system is quoted by the manufacturer at 0.5 ms. The compressed air was metered with a variable area flowmeter (Lab-Crest 448118) with a sapphire ball. The air flow rate was kept between 10 and 40 cm^3/min.

The flowmeter, pressure transducer, and bubbler tube were connected to a metal tee, with the tube to the pressure transducer aligned vertically above the bubbler tube and with the air supply through the flowmeter

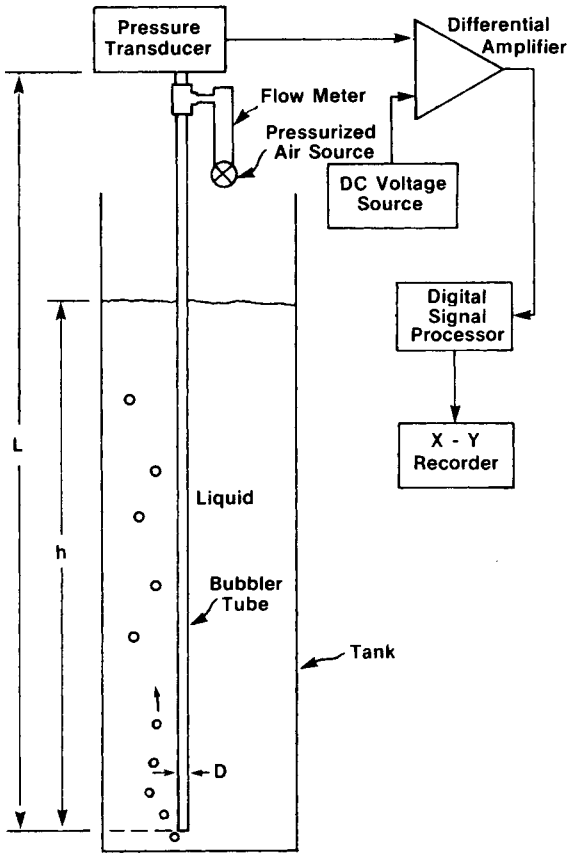

Figure 1. A schematic diagram of the experimental equipment shown for bubbler tube lengths up to 3.66 m. The setup for longer lengths was identical except a coil of hard plastic tubing was inserted between the straight metal tube and the tee connection to the pressure transducer and flow meter.

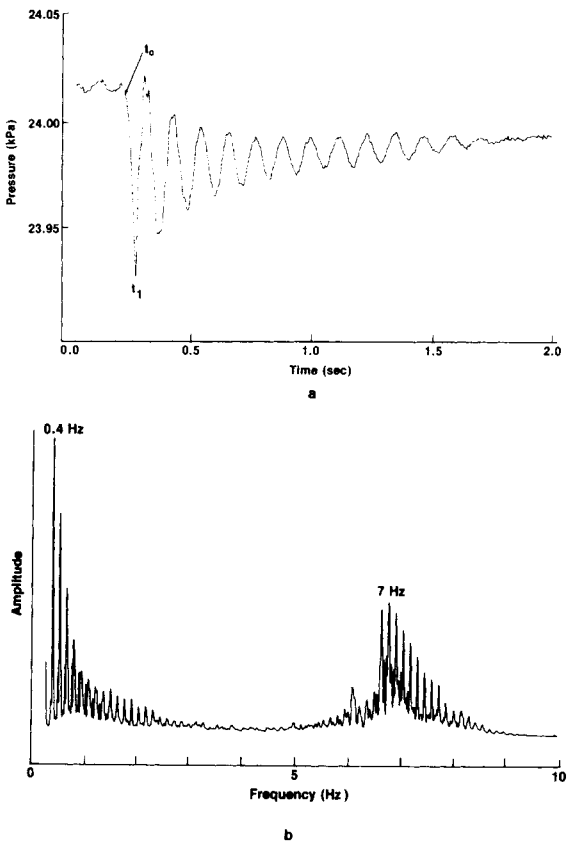

Figure 2a. The transient pressure oscillations in a 1.91 cm diameter 3.66 m long tube following a bubble breakoff at time t_o. The pressure in the tube relative to the atmosphere is about 24 kPa. The transient has been averaged over 32 bubbles. 2b. A Fourier transform of the pressure signal shown in Figure 2a. The bubbling frequency is 0.4 Hz, while the transient pressure oscillation has a frequency of about 7 Hz. Multiple peaks (spaced 0.4 Hz apart) appear at about 7 Hz because the pressure oscillation is modulated by the bubbling frequency.

entering the horizontal branch of the tee. The pressure signal from the electronic module was fed into a differential amplifier (Tektronix AM502) which amplified the signal relative to a constant voltage supplied by a precision voltage source (Analogic AN3100). Finally, the amplified signal was fed into a digital signal processor (Spectral Dynamics SD360).

All of the tube lengths were determined with a meter stick. None of the observed effects were strong functions of the tube length, so that greater accuracy was not necessary. The total tube length, including fittings, is known to within 2.5 cm. The length of the plastic tubing is known to within 1.5 cm. All of the pressure traces recorded are averages over many bubbles, usually 32. The frequency measurements were done by taking a Fourier transform of the pressure signal. The accuracy of the quoted frequencies is about 5%.

EXPERIMENTAL RESULTS

The observed time dependence of the air pressure is a superposition of two main components: damped oscillations, which are related to the response of the bubbler tube to a bubble breakoff, and the slow pressure buildup in the tube during the bubble growth. The two processes are described separately in the following subsections.

Damped Oscillations

Following a bubble breakoff the pressure in the tube has a characteristic damped oscillation, a typical example of which is shown in Figure 2a. The first pressure dip at time t_o, and the following rise at time t_1, are due to the bubble breakoff process and the subsequent inrush of the water. This can be inferred from the time intervals which are independent of tube length, tube width, and air pressure. The frequency of the damped oscillation is determined from the Fourier transform of the pressure signal; a typical example is shown in Figure 2b which corresponds to the pressure signal in Figure 2a. The frequency at 0.4 Hz corresponds to the bubbling rate while the damped oscillations occur at 7 Hz.

As a preliminary step, data was taken to determine the effect on the pressure signal of the trandsducer connection and the tilt of the bubbler tube. A 60-cm glass tube (0.95 cm o.d.) was used in this measurement since it was much easier to manipulate. A connection was tried in which the transducer and the flowmeter were aligned horizontally, while the tube was perpendicular and vertical. The oscillatory pressure signal was attenuated although the frequency remained unchanged. Thus, although the amplitude of the pressure oscillation is a sensitive function of transducer termination, the frequency is not sensitive to termination.

The 60-cm glass bubbler tube was tilted 10 degrees relative to the vertical. The pressure signals for the vertical and tilted case show that the amplitude of the oscillations varies with tilt, but the frequency is not sensitive to tilt.

Data was taken to study the dependence of the pressure signal on tube length and water height. The frequency of the oscillation is a function of tube length. The longer the tube, the slower the oscillation. In addition, the number of possible frequencies that can exist simultaneously increases with tube length. For a short tube there is only one mode of oscillation. As the

TABLE 1. EXPERIMENTAL FREQUENCIES

Tube	Diam. (cm)	End Shape	Length (m)	1st Mode (Hz)	2nd Mode (Hz)
glass	0.95	flat	0.5	38 ± 2	
glass	0.95	flat	1	31 ± 2	77 ± 7
steel	0.95	flat	3.66	16 ± 2	43 ± 4
steel	0.95	flat	7.4	10 ± 2	
glass	0.95	slanted	0.5	44 ± 2	
glass	0.95	slanted	0.8	37 ± 2	
steel	0.95	slanted	3.66	11 ± 2	
steel	0.95	slanted	7.6	8 ± 2	
steel	0.95	slanted	9.7	7 ± 2	
steel	1.91	slanted	3.66	7 ± 1	

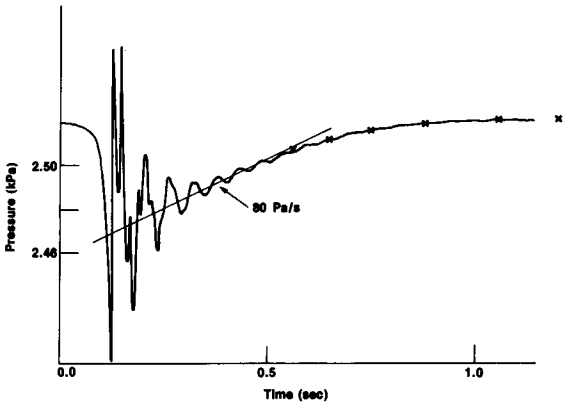

Figure 3. Pressure oscillations following bubble breakoff from a 0.96 cm diameter tube 3.66 m long. The signal is a superposition of two frequencies 16 ± 2 Hz and 43 ± 4 Hz. The transient has been averaged over 16 bubbles. The straight line corresponds to the expected linear increase in pressure as the meniscus travels down the tube. The crosses indicate the theoretically calculated pressure variation during the growth of the bubble at the end of the tube.

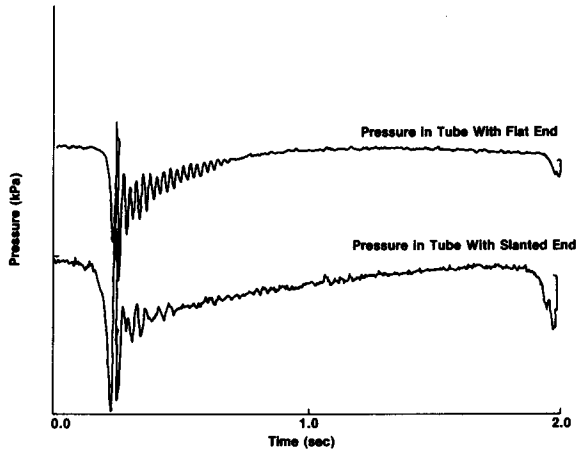

Figure 4. Pressure in tubes with different ends. The pressure in a tube with a flat end (top trace) stays constant for a large portion of the time between bubble breakoff; the pressure in a tube with a slanted end (bottom trace) increases linearly during most of the time between bubble breakoff. The pressure and time scales are the same for both curves.

tube length is increased, two things happen. The frequency of the first oscillatory mode decreases, and a new oscillatory mode appears at a higher frequency. A transient with two oscillations is shown in Figure 3. The signal for a longer tube (7.4 m) does not have easily distinguishable oscillations; rather it appears as a superposition of many frequencies. The measured frequencies for various tube lengths and tube diameters are summarized in Table 1, which shows two frequencies when two modes exist.

Measurements were also performed to study the effect of absolute pressure in the bubbler tube on the oscillation frequency. The pressure variation was obtained by changing the liquid height. No change in the frequency could be detected with a change of pressure from 2.6 kPa to 24.3 kPa. Thus, the frequency of oscillation depends on the length of the tube but is not a sensitive function of the absolute pressure in the tube.

Slow Pressure Increase

The previous discussion was concerned with the oscillatory response of the bubbler tube following a bubble breakoff. A second very important property of the pressure signal is the underlying slow buildup which occurs during the growth of the bubble. In Figure 4 are shown two pressure traces, one corresponding to a tube with a flat end, and one to a tube with a slanted end. From an examination of the two traces it can be inferred that the slow pressure buildup is a function of the geometry of the end of the tube. That this functional dependence exists is plausible since the pressure which exists in the tube depends on the liquid height from the surface to the lowest point of the bubble and on the curvature of the bubble at its lowest point. The lowest point and its curvature are largely determined by the evolution of the bubble, which in turn depends on tube end geometry. In the case of the slanted end, the growth of the bubble is constrained by the side of the tube. Figure 5b shows a sequence of photographs taken of a bubble growing at the end of a tube with a slanted end. The individual photographs are not separated by equal amounts of time, so they do not indicate rate of growth. Visual observations show that the linear pressure increase occurs while the bubble is growing up to the shape shown in the middle of the three photographs. The rest of the development is very rapid and leads to a bubble breakoff.

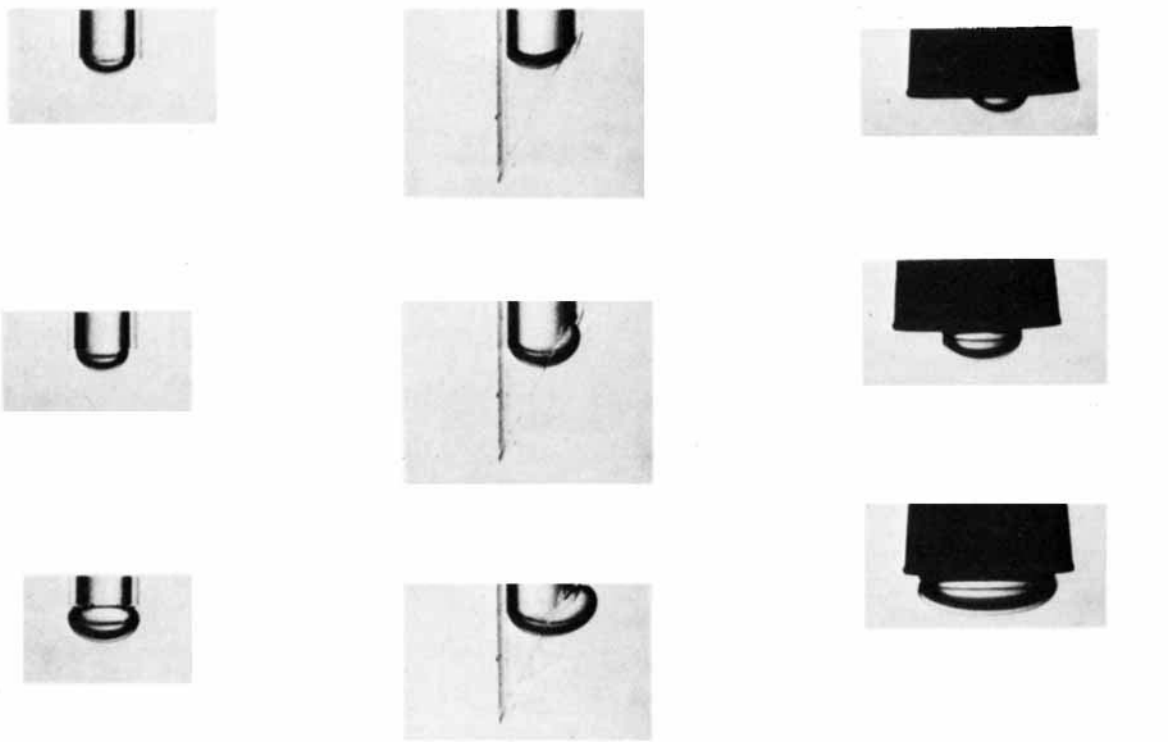

Figure 5. A sequence of photographs of a bubble growing from a tube with a) a flat end, b) a slanted end, and c) a flanged end. The experimental conditions for the sequences are identical to those for a) the upper trace in Figure 4, b) the lower trace in Figure 4, and c) the trace of Figure 6, respectively. The time intervals between photographs are not uniform.

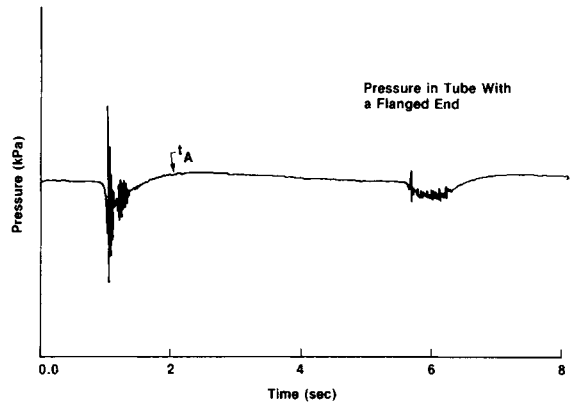

Figure 6. Pressure in a tube with a flanged end. The pressure climbs to a maximum value at time t_A and then decreases linearly for the major portion of the time between bubbles.

In the case of a tube with a flat end, the evolution of the bubble is much more symmetrical as can be seen in Figure 5a, which shows a sequence of photographs taken of a bubble growing at the end of a tube with a flat end. Visual observations show that the bubble grows axially or vertically to some maximum dimension and then expands horizontally. This growth is reflected in the pressure signal which is characterized by a rapid pressure rise followed by a relatively long period during which the pressure increases slowly to the breakoff level. If a flange is provided at the flat end of the tube, the bubble develops as shown in the sequence of photographs in Figure 5c. The corresponding pressure variation in the bubbler tube is shown in Figure 6. By correlating visual observations with the pressure trace it is apparent that up to point t_A in Figure 6, the bubble grows while it is attached to the edges of the tube. During this phase of the growth the bubble size increases axially and thus the pressure increases. Beyond point t_A, the edge of the bubble breaks away from the inner surface of the tube and continues its growth attached to the flat surface surrounding the edge. The sequence of photographs shown in Figure 5c demonstrates that the edge of the bubble breaks away from the inner surface of the tube and moves horizontally outward along the flange. As a result, the vertical height of the bubble does not increase very much in proportion to its volume increase. Secondly, the curvature of the bubble at its lowest point decreases as the bubble grows in the horizontal dimension. Both of these effects, the slow height variation and the decrease of curvature, are consistent with the pressure trace shown in Figure 6 in which a pressure decrease is observed in the later stage of the bubble development.

In summary, the slow variation of the pressure in the bubbler tube reflects the evolution of the bubble shape, which in turn depends strongly on the geometry of the end of the tube.

THEORETICAL DISCUSSION

In the following, a theoretical analysis of the damped pressure oscillations and the slow pressure increase in the bubbler tube is given. The prediction of the oscillation frequencies compares favorably with the experimental values. The predicted increase of pressure due to bubble growth at the end of a tube with a flat end is also in agreement with the observed pressure variation.

Damped Oscillations

The air pressure oscillations following the release of a bubble were visually observed to be coincident with oscillations of the liquid level inside the tube. Thus, the oscillations can be analyzed only by considering the composite system consisting of the air in the tube and the liquid outside the tube and inside it at the lower end. The flow of air into the tube is assumed to be sufficiently slow that its effect need not be considered; pressure oscillations about a constant average pressure are described.

To simplify things, consider an oscillation at just one frequency, $\omega/2\pi$. Since the system is linear for small amplitudes, more general oscillations can be obtained by superposition. The frequency is sufficiently low that the wave length of the associated sound wave is very large compared with the tube diameter. So only the fundamental sound mode propagates in the tube, and this mode is a plane wave. Thus, the pressure P and the velocity u of the air depend only on the longitudinal coordinate x and the time t. They are related by the inviscid momentum equation

$$\rho_a \, \partial u/\partial t = -\partial P/\partial x, \tag{1}$$

which applies because viscosity has a negligible effect on the frequency of oscillation. This equation will also be used to obtain the boundary conditions at the end of the tube.

Assuming that the air pressure in the tube consists of a constant term plus two waves, one travelling up from the open lower end of the tube, and the other travelling down toward it, Eq. 1 can be solved for u with the result

$$u = \frac{P_1}{\rho_a c} \sin\left(\omega \frac{x-L}{c}\right) \sin(\omega t). \tag{2}$$

At the liquid surface (at $x = 0$), Eqs. 1 and 2 give

$$\partial P/\partial t = \omega \rho_a c u \cot(\omega L/c). \tag{3}$$

The forces on the surface between the air and water are due to the hydrostatic pressure of the liquid pushing up and the static plus acoustic pressure of the air pushing down; surface tension is assumed negligible. The resulting equation of surface motion is

$$M \frac{du}{dt} = A\,[\rho_\ell g\,(h-\xi) - P], \tag{4}$$

Equation 4 can be seen to be just the Bernoulli equation at the air-liquid surface (Kinsman, 1965)

$$\partial\phi/\partial t = g(h-\xi) - P/\rho_\ell. \tag{4'}$$

To see it, choose the arbitrary function of time that can be added to the liquid velocity potential ϕ so that $\phi = \ell u$ at the surface. (Note that ϕ/u at the surface is also constant in the usual treatment of surface waves.) Here

$$\ell = M/\rho_\ell A \tag{5}$$

is the (constant) average length of the liquid column in the tube plus a correction for the virtual mass of the liquid outside. Inserting $\phi = \ell u$ into Eq. 4 and using Eq. 5 leads to the Bernoulli relation (Eq. 4') for the air-liquid surface.

The equation for the frequencies of oscillation can be obtained by differentiating Eq. 4 with respect to time, applying Eqs. 2, 3, and 5, and dividing by u to get

$$\ell\,\omega^2 - \frac{\omega\rho_a c}{\rho_\ell}\cot\left(\frac{\omega L}{c}\right) - g = 0. \tag{6}$$

By use of the quadratic formula, Eq. 6 can be rewritten as

$$\omega = \left[\frac{g}{\ell} + \frac{c^2\rho_a{}^2}{4\rho_\ell{}^2\ell^2}\cot^2\left(\frac{\omega L}{c}\right)\right]^{1/2} + \frac{c\rho_a}{2\rho_\ell\ell}\cot\left(\frac{\omega L}{c}\right) \tag{7}$$

In the general case, Eq. 7 can be solved only numerically. To do this, a value for ℓ is needed. In principle, the length ℓ, or equivalently the virtual mass M, can be obtained by solving for the liquid velocity potential field ϕ subject to the appropriate boundary conditions. The virtual mass can then be obtained from the value of ϕ at large distances. In the treatment below, ℓ will be considered a parameter and chosen to give the best estimate of the experimentally measured frequencies.

For our experiments, the liquid is water and the air is at standard conditions so $c = 331.78$ m/s, $\rho_a/\rho_\ell = 0.001293$, and $g = 9.8$ m/s^2. Table 2 contains calculated values of the parameter ℓ for some of the experimental frequencies in Table 1; the calculation was done using Eq. 6. Given the large uncertainty in the values of ℓ, the observed frequencies in Table 2 are consistent with a single value of the parameter ℓ, equal to about 4 mm. Figure 7 summarizes the experimental frequencies for a tube with a flat end and those calculated for various values of L using Eq. 7. On the basis of Table 2, the parameter ℓ was set to 4 mm to get a reasonable overall correspondence between the theoretical curve and the experimental values. The frequency depends strongly on the value of the tube length L, and there is only a small discrepancy for smaller

TABLE 2. CALCULATED VALUES OF THE PARAMETER ℓ

L(m)	$\omega/2\pi$ (Hz)	ℓ (mm)
	36	5.54
0.5	38 ± 2	4.95
	40	4.44
	29	4.14
1.0	31 ± 2	3.57
	33	3.10
	19	4.79
2.0	21 ± 2	3.75
	23	2.97
	70	1.88
2.0	77 ± 7	3.91
	84	20.37
	14	4.61
3.66	16 ± 2	3.09
	18	2.04
	39	3.90
3.66	43 ± 4	9.90
	47	12.57

values of L. This may not be significant because, for $L \leq 1$ m, a glass tube was used, while for larger values of L a stainless tube was used.

Measurements indicate that the frequency depends on the geometry of the bubbler tip and on the diameter of the tube. Table 3 lists the parameter ℓ for measured frequencies for several different bubbler tip configurations and two bubbler diameters. In all cases the length of the tubes was held constant at 3.66 m. The value of ℓ increases from 3 to 9 mm when the tube end is tapered; it further increases by a factor of 1.8 from 9 to 16 mm when the diameter of the tube is doubled from 0.95 to 1.91 cm. The general trend is that as the area of contact between the air and water increases, the effective mass of water participating in the motion increases.

The solution for ω is not very sensitive to variation in the air density ρ_a. For example, increasing ρ_a by 20% increased the calculated frequency from 18.5 to 19.8 Hz, a 5% change. During the measurements the pressure in the tube varied by about 17%; the variation was caused by changes in the height of the liquid above the bottom end of the tube. Assuming that the air density depends linearly on the pressure, we expect that the air density in the tube varied by about 17%. The theory predicts that a 17% change in air density leads to a frequency change which is less than 5%. Since the experimental error in frequency measurement is of the order of 5%, it can be concluded that the theory is consistent with the observed lack of dependence of the oscillation frequency on air density.

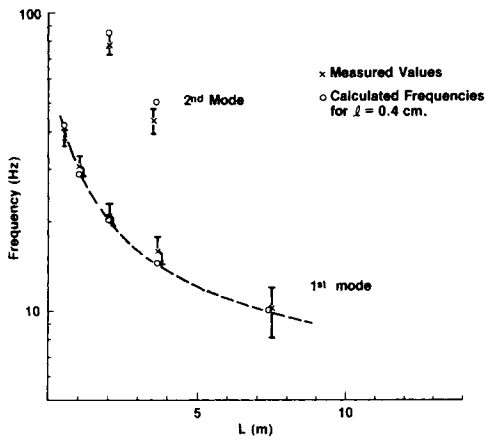

Figure 7. A comparison between observed and calculated frequencies of oscillations in tubes following a bubble breakoff. Results are shown as a function of tube length for flat ended tubes. For the tubes of length 2 m and 3.66 m, a comparison is made for the first and second mode of oscillation.

TABLE 3. PARAMETER ℓ FOR MEASURED FREQUENCIES

Tube Diameter (cm)	End Geometry	f[Hz]	ℓ[mm]	M[g]
0.96	flat	16	3	0.2
0.96	tapered	11	9	0.6
1.91	tapered	7	16	5.0

Tube length is 3.66 m.

In addition to the motion discussed above in which the water level moves up and down, there are the normal modes of vibration of the air-water surface in the cylindrical container. The lowest mode is a deformation in which the air-water surface seesaws about a stationary level. The estimated frequency of this motion is on the order of 10 Hz. The seesaw mode can be excited if the initial water surge is unsymmetrical, that is if it comes in faster at one side of the tube than the other. Such an asymmetry is always present due to the asymmetry of bubble release. The lowest order axially symmetric normal mode has a frequency on the order of 80 Hz. It can be excited during the initial surge of water since it couples to the up and down motion of the surface. The coupling is via the adherence of the water to the sides of the tube; as the air-water surface moves, the water in contact with the walls will be slowed down relative to the water in the center of the tube, thus leading to a surface deformation. However, none of these modes will induce pressure variation in the tube since for all of them the average displacement of the surface is zero.

Slow Pressure Increase

When a bubble breaks off the end of the tube, enough air is carried away in the bubble that the average position of the air-water interface is initially a small distance above the end of the tube. As air continues to enter the tube from the top, the average position of this surface is caused to move down the tube and grow into a new bubble. This is associated with a slow increase in the average air pressure on which the oscillations are superposed.

In order to predict the time dependence of this slow increase, we use the gas law, which relates the air pressure P to the total volume V of air in the tube and bubble. Let $\dot{n}$ be the number of moles of air flowing into the tube and bubble per unit time. Since $\dot{n}$ is very nearly constant, PV is very nearly linear in time t. Let P_o be the pressure, V_o be the volume, and $t = 0$ be the time when the air-water surface is at the end of the tube. Then if we subtract the gas equation at time $t = 0$ from the equation at time t, we get

$$PV - P_oV_o = \dot{n}RTt, \tag{8}$$

where R is the universal gas constant, and T is the absolute temperature. Now $\dot{n} = \rho_aQ/m$, where ρ_a is the density of the air, Q is the volume flowrate into the tube and bubble, and m is the mass per mole of air. But $\rho_a/m = P/RT$, so the right side of Eq. 8 is just PQt. Let $P_1 = P - P_o$, $V_1 = V - V_o$, and use these to substitute for P and V in Eq. 8. Note that after a bubble has broken off $P_1 \ll P_o$ so that the P_1V_1 term can be neglected, and P can be replaced with P_o on the right, with the result that

$$P_1V_o + P_oV_1 = P_o\,Qt. \tag{9}$$

Here $P_1 > 0$ and $V_1 > 0$ for $t > 0$, and $P_1 < 0$ and $V_1 < 0$ for $t < 0$.

The pressure dependence for $t < 0$, i.e., before the air-water interface gets down to the end of the tube, can be predicted regardless of the shape of the end of the tube. Prior to that time, the distance between the interface and the end of the tube is $-V_1/A$, which is >0 since $V_1 < 0$. Since the difference in hydrostatic pressures $P_o - P = -P_1$ must equal $\rho_\ell g$ times this distance, we have

$$V_1 = P_1A/\rho_\ell g, \tag{10}$$

where P_1 is also <0. When this is used to eliminate V_1 in Eq. 9 and

the equation is solved for P_1, the result is

$$P_1 = \frac{P_o Q}{V_o + P_o A/\rho g}\, t. \tag{11}$$

This is valid from the time the last bubble has broken off until the air-water interface reaches the end of the tube. Of course, the oscillatory pressure must be added to this result in order to get the observed time dependence.

The pressure dependence for $t > 0$ depends on the shape of the end of the tube. In the case of a tube with a slanted end, the observed pressure growth remains mostly linear, which indicates that Eq. 10 remains approximately valid also for $t > 0$.

For tubes with a flat end the pressure variation is characterized by a rapid increase followed by a long period of relatively stable pressure. The observed pressure change is consistent with the result of a calculation of the shape of an axisymmetric bubble growing at the end of the tube.

The calculation was performed using a differential equation equivalent to the one given by Bashforth and Adams (1883):

$$\begin{aligned} &R^3 \ddot{R} + \dot{R}^4 + (R^2 + \dot{R}^2)\, R \dot{R} \cot\theta \\ &- (P_o - P + \rho g R \cos\theta)\,(R^2 + \dot{R}^2)^{3/2} R^2/\sigma \\ &- (R^2 + \dot{R}^2)\,(2R^2 + \dot{R}^2) = 0. \end{aligned} \tag{11}$$

Here the origin of the coordinate system is at the center of the circle forming the bottom edge of the bubbler tube. $R(\theta)$ is the distance from the origin to the bubble surface, and θ is the angle between R and the vertical line passing through the origin. $\dot{R}$ and $\ddot{R}$ are derivatives of $R(\theta)$ with respect to the angle θ. Equation 11 can be derived in a very instructive way by using variational techniques. Form the expression for the work done in establishing the volume and surface of the bubble. Next minimize this work keeping the volume of the bubble fixed. Equation 11 is just the Euler-Lagrange equation for the shape $R(\theta)$ of the bubble for which the work is minimum. The Lagrange multiplier P is equal to the pressure at the bottom of the bubble tip given by the Laplace formula

$$P = P_o + \rho g L + 2\sigma\kappa \tag{12}$$

(See e.g. Landau and Lifshitz, 1959) where $L = R(0)$ and

$$\kappa = \frac{L - [\ddot{R}]_{\theta=0}}{L^2} \tag{13}$$

is the radius of curvature at the bottom of the bubble.

The bubble growth calculation was performed numerically by setting the bubble height to a constant and finding the value for P such that the bubble terminates on the end of the tube. The derivative $dR/d\theta$ at the end of the tube was not constrained. Physically, this derivative determines the angle between the bubble surface and the tube wall. Since this angle is fixed by the values of various surface tensions σ_{LS}, σ_{LV}, and σ_{SV}, it may appear improper to let the angle vary in the calculation. However, the end of the tube is rounded and its walls are of finite thickness so that within limits, the values of $dR/d\theta$ are practically unconstrained.

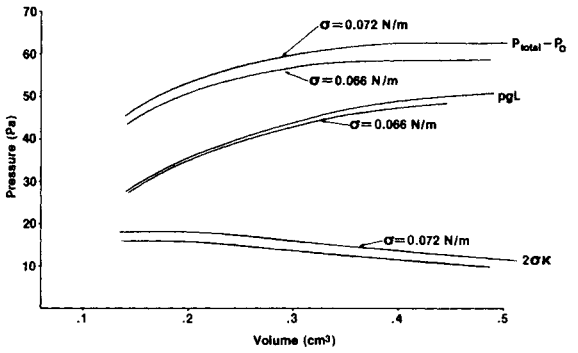

Figure 8. The results of the bubble growth calculation. The top curve is the total pressure in the tube less the hydrostatic pressure at the lower end of the tube as a function of bubble volume. The middle curve shows the contribution to the pressure due to the hydrostatic pressure ρgL, where L is the height of the bubble. The bottom curve shows the contribution due to surface tension. The three pressures are calculated for two values of surface tension: 0.072 N/m for water at 20°C, and 0.066 N/m for water at 60°C.

The results of the calculation are shown in Table 4 and Figure 8. They were performed for a tube diameter of 1 cm and water surface tensions of 0.072 and 0.066 N/m corresponding to temperatures of 20 and 60°C, respectively (Padday, 1969). Figure 8 shows a plot of the pressure inside the tube relative to the pressure at the bottom tip of the tube.

Two contributions to the pressure are identified in Eq. 12. The hydrostatic pressure ρgL due to the downward extension of the bubble, and the additional pressure $2\sigma\kappa$ needed to "stretch" the bubble surface. The two contributions are plotted separately in Figure 8. The ordinate is the volume V_1 of the bubble. The calculation shows that after a period of increase, the pressure in the tube becomes constant as a function of bubble volume. This is because the increase in hydrostatic pressure due to bubble growth is offset by the decrease in the pressure due to the decrease of surface curvature.

The maximum pressure variation is about 61 Pa, a value consistent with the observed pressure variation during bubble breakoff. A calculation with $\sigma = 0.066$ N/m was performed to determine the sensitivity of the maximum pressure to the surface tension σ. In a change of σ from 0.072 to 0.066 N/m the maximum pressure dropped by approximately 4 Pa. Some of this was due to change in $2\sigma\kappa$, and some due to the greater horizontal growth possible with smaller surface tension.

The calculation points to the importance of surface tension in tank volume measurements where the calibration is usually done with water, while the actual volume measurements are carried out with a liquid of a different surface tension. The sensitivity of the pressure measurement to σ may be reduced by using a tube of larger diameter. For example, for a tube of radius = 0.7 cm the hydrostatic and surface tension contributions are 39.1 and 9.0 Pa, respectively, for bubble length of 0.4 cm and 48.9, and 7.8 Pa for

TABLE 4. RESULTS OF THE CALCULATION

Surface Tension = 0.072 N/m L(cm)	Vol. (cm³)	$P - P_o$ (Pa)	ρgL (Pa)	Tube Radius = 0.5 cm $2\sigma\kappa$ (Pa)
0.30	0.1515	47.3	29.3	18.0
0.35	0.1904	52.2	34.2	18.0
0.40	0.2386	56.4	39.1	17.3
0.45	0.3028	59.8	44.0	15.8
0.50	0.3975	62.5	48.9	13.6
0.52	0.4788	62.5	50.8	11.7
Surface Tension = 0.066 N/m				
0.30	0.1533	45.3	29.3	16.0
0.35	0.1933	50.1	34.2	15.9
0.40	0.2454	54.1	39.1	15.0
0.45	0.3138	57.5	44.0	13.5
0.475	0.3619	58.9	46.4	12.5
0.50	0.4448	59.4	48.9	10.6

bubble length of 0.5 cm. Thus, the ratio of hydrostatic to surface tension contribution is about 5, while in the case of the 0.5 cm radius tube, the same ratio is about 3.

The results of the above discussion were used to calculate the pressure variation with time for the experimental situation shown in Figure 3. The values of the parameters that apply in Figure 3 are, $V_o = 184\ \text{cm}^3$, $P_o = 1.027 \times 10^5$ Pa, $Q = 33\ \text{cm}^3/\text{min}$, $V_o/A = 366$ cm. Substituting into Eq. 12, and using $\rho_\ell \simeq 1\ \text{g/cm}^3$ and $g = 980\ \text{cm/s}^2$, we get $P_1/t = 80$ Pa/s. This result is in agreement with the experimental pressure variation of about 80 Pa/s as determined from the straight line in Figure 3. Where the straight line deviates from the pressure trace, the pressure variation can be obtained by substituting V_1 as a function of P_1 from Table 4 into Eq. 9 to get the corresponding time. The first pair $V_1 = 0.1515\ \text{cm}^3$ and $P_1 = 47.3$ Pa is made to coincide with the experimental trace at the approximate location where the straight line diverges from the experimental trace. In effect this defines $t = 0$, the time at which the liquid level has reached the end of the tube and the bubble commences to grow. The other five calculated points are plotted in Figure 3 relative to the first point. The correspondence between the observed and expected pressure variation is good.

ACKNOWLEDGMENTS

The authors are grateful to the following persons for the help they provided during the experiment and the preparation of the manuscript. We thank George E. Mattingly for a critical reading of the manuscript and many suggestions for improving it, G. Paul Baumgarten for setting up the equipment and general assistance, David G. Cooper for help in construction of electronics, V. Brame for taking the photographs, and S. R. Coriell and M. R. Cordes for helpful discussion concerning the bubble growth calculation.

NOTATION

A = cross-sectional area of the bubbler tube
c = speed of sound in air
g = acceleration due to gravity
h = average difference in height between the air-liquid surface outside and inside the bubbler tube
L = length of the bubbler tube; distance of the lowest point of the bubble from the end of the bubbler tube
M = virtual mass of the liquid participating in the oscillatory motion of the air-liquid surface inside the bubbler tube
$\dot{n}$ = number of moles of air per unit time flowing into the bubbler tube
P = total pressure in the bubbler tube
P_o = pressure in the bubbler tube when the air-liquid surface is at the end of the tube
P_1 = amplitude of pressure waves in the bubbler tube; $P - P_o$
Q = volume flow rate into the bubbler tube
R = universal gas constant
$R(\theta)$ = polar coordinate defining the shape of a bubble
T = absolute temperature of the air inside the bubbler tube
t_o = time at which a bubble starts to break off from the end of the bubbler tube
t_1 = time at which the first minimum of pressure occurs following the bubble break off
u = axial velocity of air in the bubbler tube
V = volume of air in the bubbler tube
V_o = volume of air in the bubbler tube when the air-liquid surface is at the end of the tube
V_1 = $V - V_o$; volume of air inside a bubble
ϕ = velocity potential of the liquid
κ = curvature at the lowest point of the bubble
ρ_a = density of air
ρ_ℓ = density of liquid
σ = surface tension
ξ = height of the air-liquid surface inside the bubbler tube relative to the average height h
ω = angular frequency of oscillations inside the bubbler tube

LITERATURE CITED

Bashforth, F., and J. C. Adams, *Capillary Action*, Cambridge University Press (1883).

Davies, W., P. T. Good and A. G. Hamlin, "A Statistical Examination of the Practical Problems of Measurement in Accountancy Tanks," *Nuclear Safeguards Technology*, **II**, IAEA-SM-231/95, Vienna, p. 593 (1979).

Jones, F. E., "Application of an Improved Volume Calibration System to the Calibration of Accountability Tanks," *Nuclear Safeguards Technology*, **II**, IAEA-SM-231/95, Vienna, p. 653 (1979).

Kinsman, B., *Wind Waves*, Prentice-Hall, Englewood Cliffs, NJ, p. 112 (1965).

Landau, L. D., and E. M. Lifshitz, *Fluid Mechanics*, Pergamon Press, London, p. 231 (1959).

Padday, J. F., "*Surface Tension Part I. The Theory of Surface Tension*," *Surface and Colloid Science*, **I**, ed., Egon Matijevic, p. 90 (1969).

Manuscript received February 9, 1981; revision received October 2, and accepted February 22, 1982.